Electronic Supplementary Information (ESI)

Wearable Anti-Temperature Interference Strain Sensor with Metal Nanoparticle Thin Film and Hybrid Ligand Exchange

Young Kyun Choi[a], Taesung Park[a], Dong Hyun David Lee[b], Junhyuk Ahn[a], Yong Hwan Kim[a], Sanghyun Jeon[a], Myung Joon Han[b], and Soong Ju Oh[a,]*

[a] Department of Materials Science and Engineering, Korea University, 145, Anam-ro Seongbuk-gu Seoul, 02841, Republic of Korea

[b] Department of Physics, Korea Advanced Institute of Science and Technology, 291, Daehak-ro, Yuseong-gu, 34141, Korea

E-mail: sjoh1982@korea.ac.kr

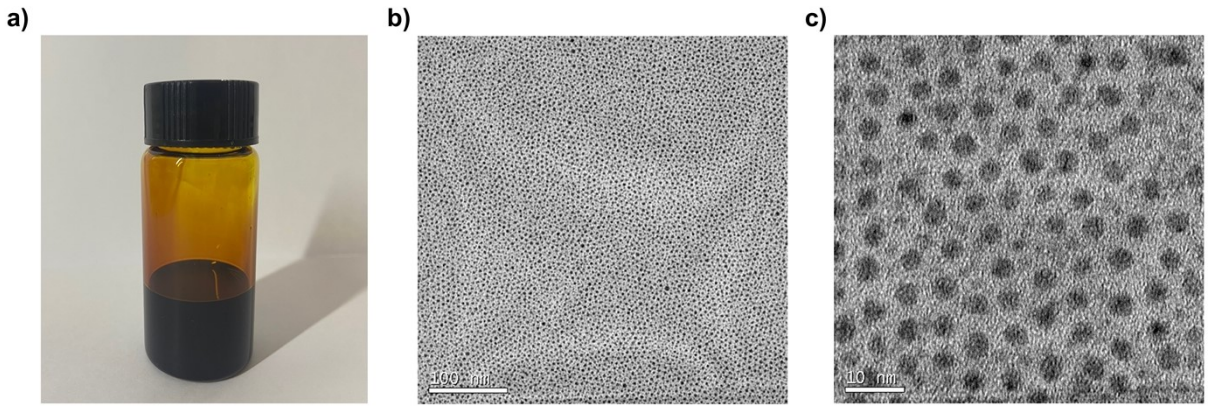

Fig. S1 (a) Image of colloidal Ag NPs, TEM image of (b) 100-nm, (c) 10-nm scale bar of 4-nm Ag NPs.

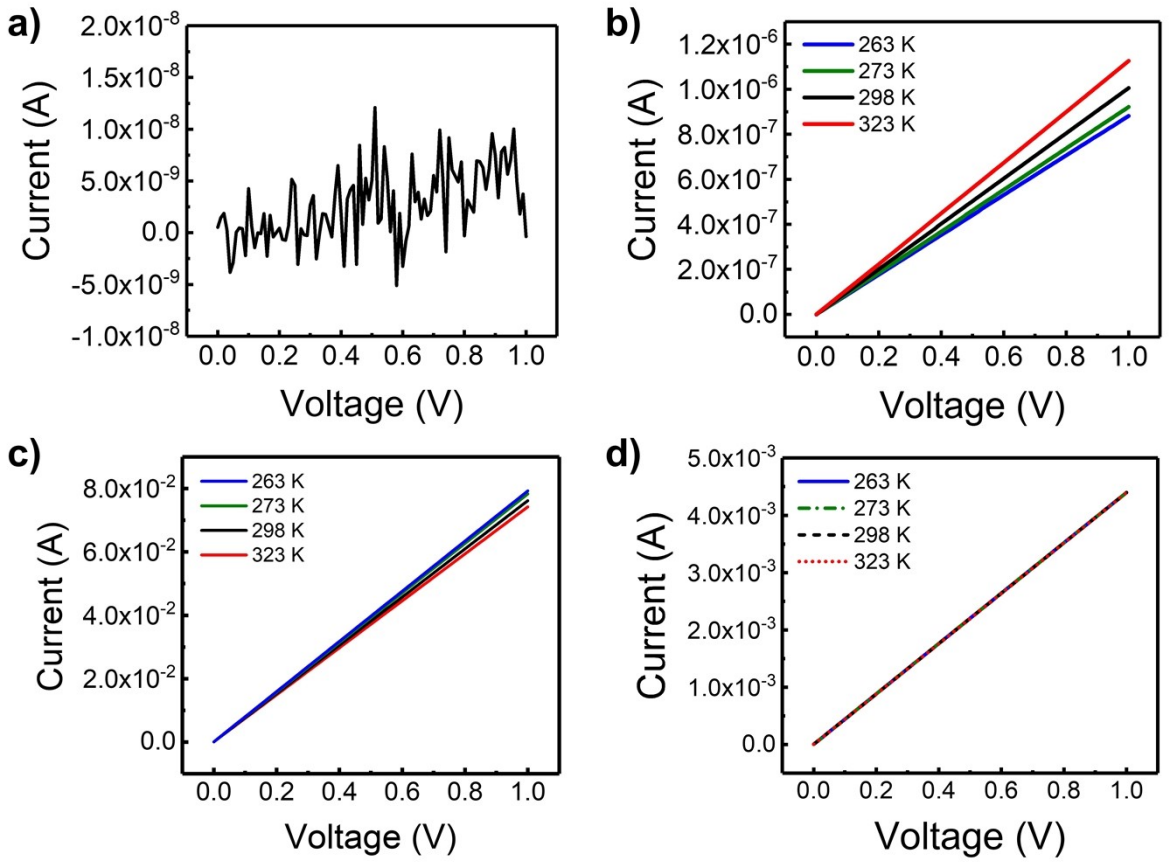

Fig. S2 I-V characteristics of the (a) as-synthesized, (b) only MPA-treated (X_{TBAB} = 0), (c) only TBAB-treated (X_{TBAB} = 1) and (d) hybrid ligand-treated (X_{TBAB} = 0.88) Ag NP thin films at 263, 273, 298 and 323 K.

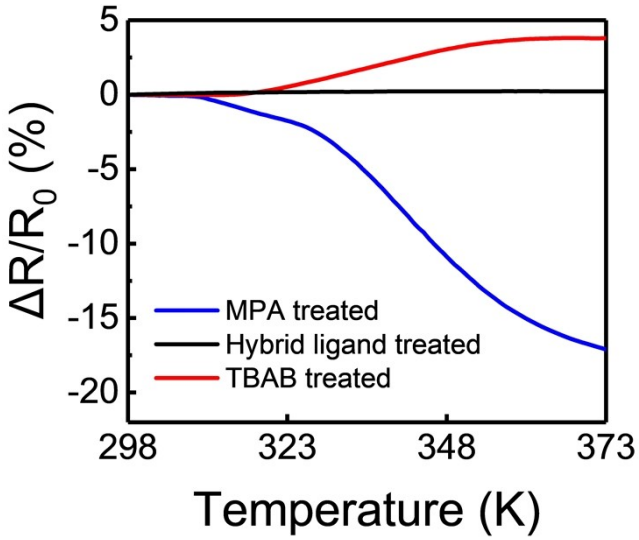

Fig. S3 $\Delta R/R_0$ vs. temperature curve of each ligand-treated Ag NP thin films, with the heating temperature increasing from 298 to 373 K

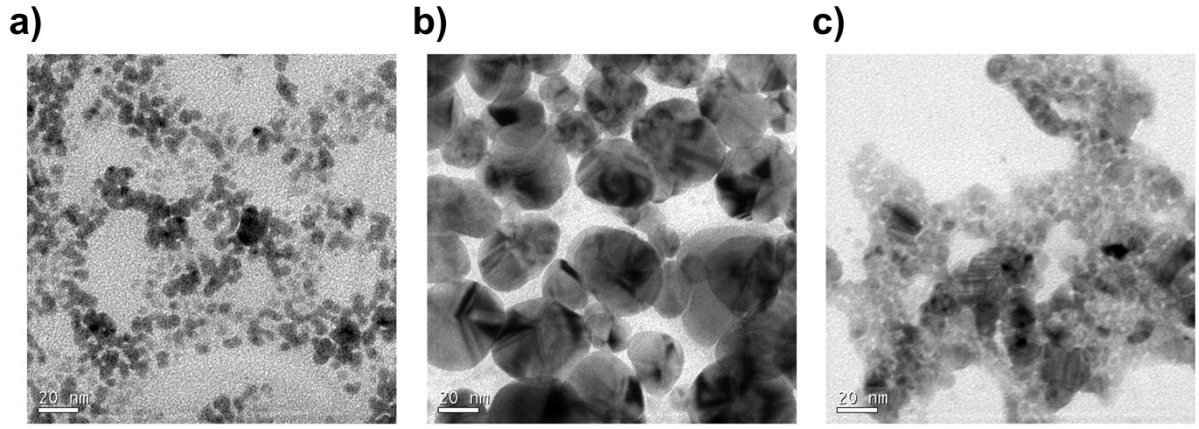

Fig. S4 TEM image of (a) MPA-treated, (b) TBAB-treated, and (c) hybrid ligand-treated Ag NPs (Scale bar = 20 nm).

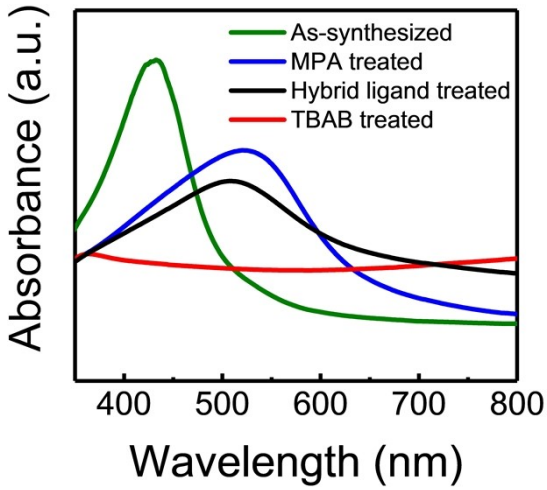

Fig. S5 UV-vis absorption spectra of the as-synthesized, MPA-treated, TBAB-treated, and hybrid ligand-treated Ag NP thin films.

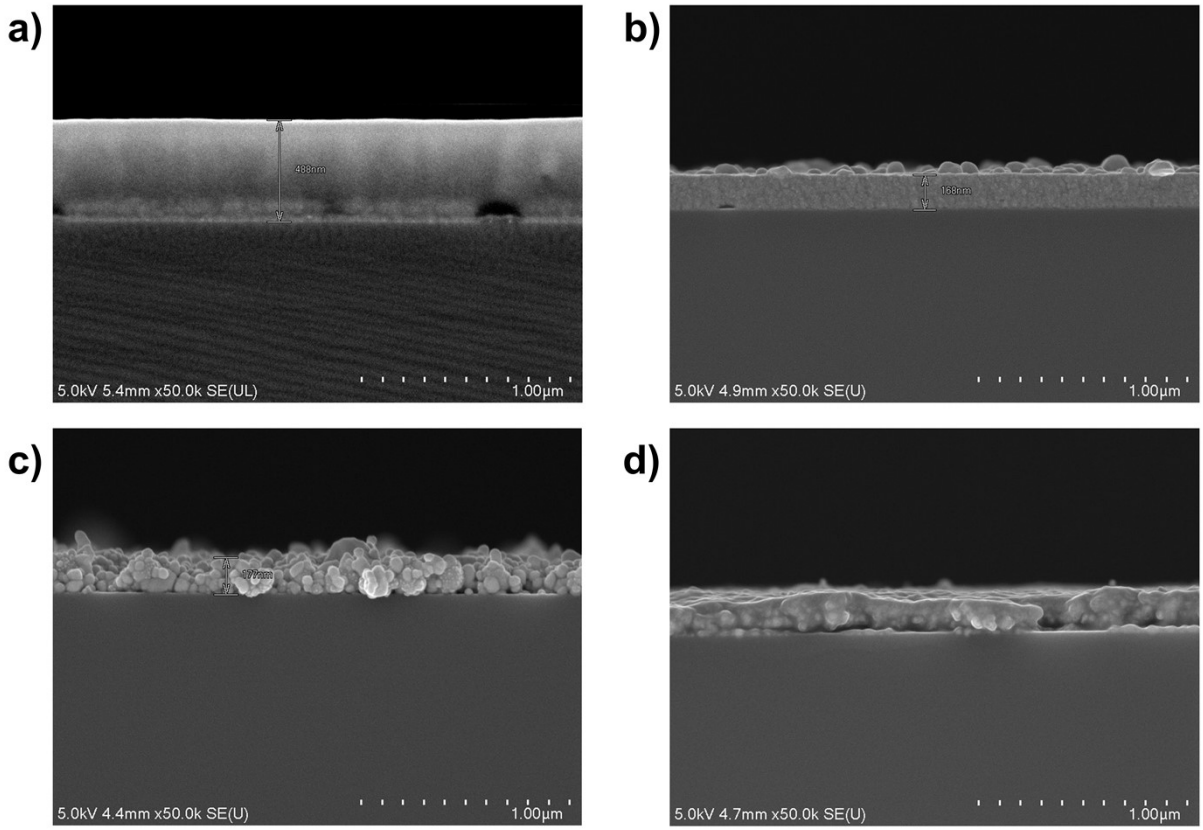

Fig. S6 Cross-sectional SEM images of the (a) as-synthesized, (b) MPA-treated, (c) TBAB-treated, and (d) hybrid ligand-treated Ag NP thin films (Scale bar = 1 µm).

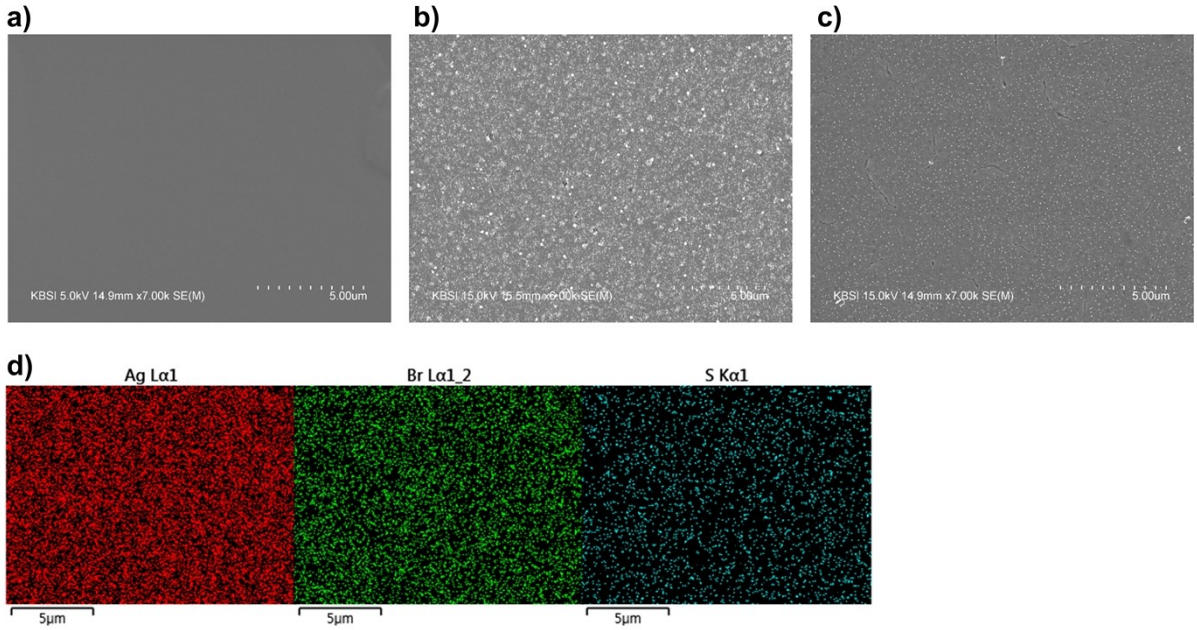

Fig. S7 SEM images of (a) MPA-treated, (b) TBAB-treated, and (c) hybrid ligand-treated Ag NP thin films, along with (d) EDS mapping of (c) (Scale bar = 5 µm).

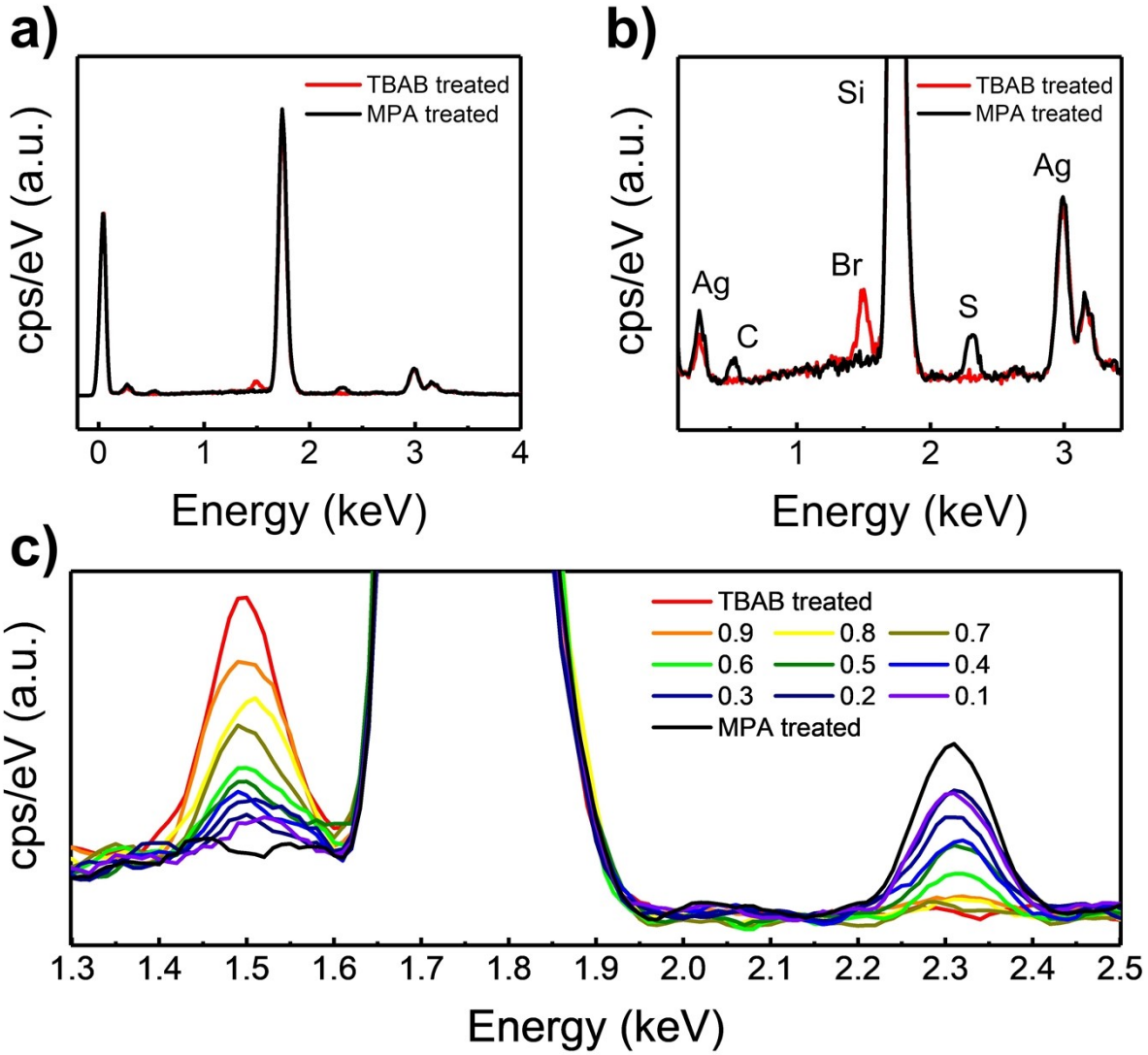

Fig. S8 EDS spectra of (a) MPA-treated and TBAB-treated Ag NP thin films, (b) magnified view of (a), (c) magnified view over the energy range from 1.3 to 2.5 keV of hybrid ligand-treated Ag NP thin films, with X_{TBAB} varied at an interval of 0.1.

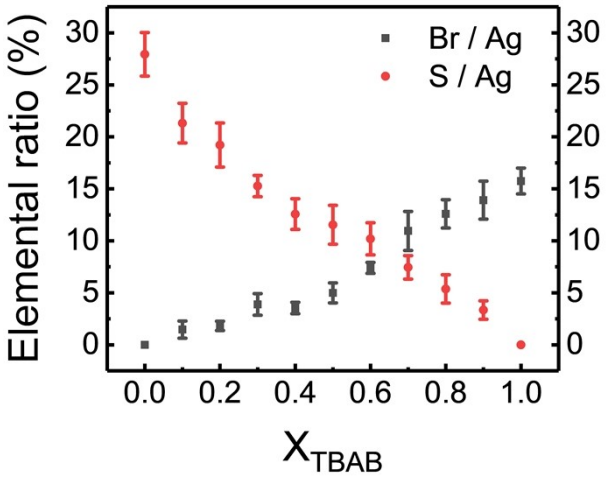

Fig. S9 Elemental ratio (Br/Ag and S/Ag) in each hybrid ligand-exchanged Ag NP thin film against X_{TBAB} obtained by EDS analysis.

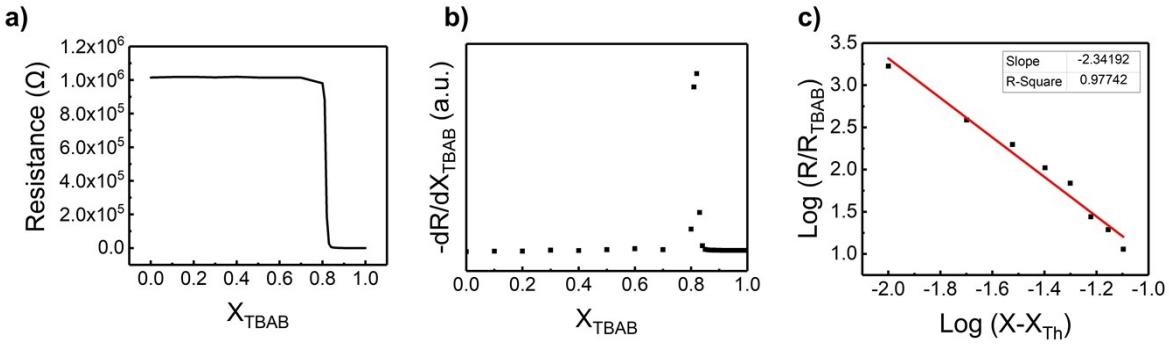

Fig. S10 Resistance curve fitting for deriving percolation threshold (X_{Th}) and critical index (t). (a) Linear curve plot of resistance against overall X_{TBAB} in hybrid ligand-exchanged Ag NP system. (b) The differential curve of (a), (c) log-log plot based on percolation threshold, X_{Th}.

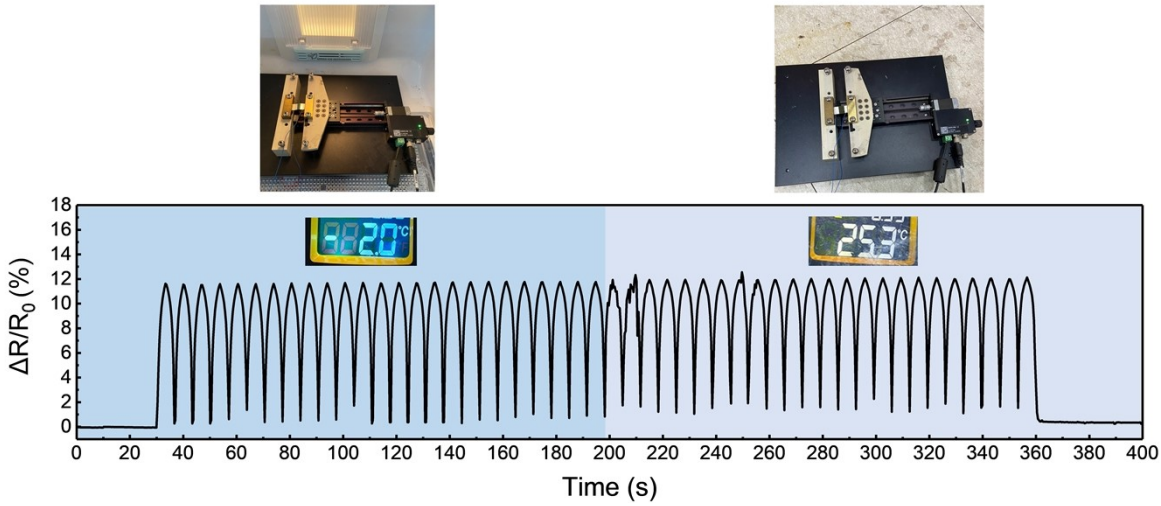

Fig. S11 Realtime $\Delta R/R_0$ – time curve of hybrid ligand treated Ag NP thin film strain sensor. The strain sensor is connected to the Jabber system and is continuously applied with a strain/release of 1.0 %. From 0 seconds to 200 seconds, a simple low temperature environment is created by placing the sensor in the freezer. After 200 seconds, the sensor is moved from the freezer to a ambient room temperature environment. Inset images are the temperature of the strain sensor measured with a digital infrared thermometer in each temperature section.

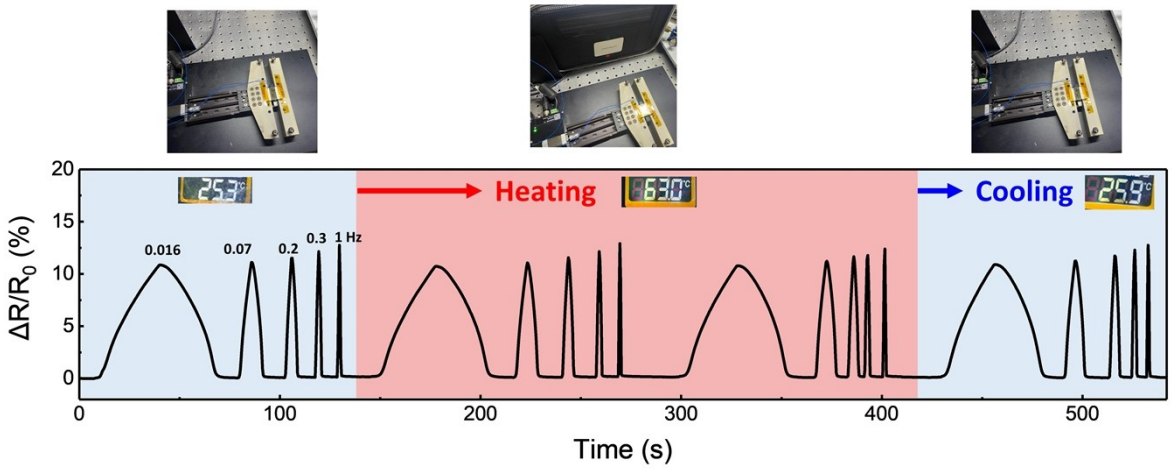

Fig. S12 Realtime $\Delta R/R_0$ – time curve of hybrid ligand treated Ag NP thin film strain sensor according to various bending frequencies and temperature fluctuations. The inset numbers 0.016, 0.07, 0.2, 0.3 and 1 are the frequencies at which the sample bends over 60, 14, 5, 3 and 1 second, respectively. Inset images are the temperature of the strain sensor measured with a digital infrared thermometer in each temperature section.

X_{TBAB}	Resistivity (Ω · cm)	TCR (K)	X_{TBAB}	Resistivity (Ω · cm)	TCR (K)
0	11.8 ± 2.1	− 4.1 ± 0.18 × 10^{-3}	0.87	1.2 ± 0.5 × 10^{-2}	− 3.2 ± 2.4 × 10^{-4}
0.1	12.2 ± 2.3	− 4.1 ± 0.22 × 10^{-3}	0.88	4.9 ± 1.4 × 10^{-3}	− 2.0 ± 5.3 × 10^{-5}
0.2	12.3 ± 1.9	− 4.2 ± 0.19 × 10^{-3}	0.89	3.4 ± 0.9 × 10^{-3}	− 8.4 ± 8.2 × 10^{-5}
0.3	12.7 ± 2.0	− 4.1 ± 0.24 × 10^{-3}	0.9	1.9 ± 0.5 × 10^{-3}	2.2 ± 1.1 × 10^{-4}
0.4	12.2 ± 2.1	− 4.1 ± 0.20 × 10^{-3}	0.91	1.6 ± 0.3 × 10^{-3}	3.6 ± 0.8 × 10^{-4}
0.5	12.8 ± 1.7	− 4.0 ± 0.23 × 10^{-3}	0.92	1.5 ± 0.3 × 10^{-3}	4.7 ± 0.9 × 10^{-4}
0.6	11.7 ± 2.5	− 4.1 ± 0.22 × 10^{-3}	0.93	1.3 ± 0.2 × 10^{-3}	5.5 ± 0.6 × 10^{-4}
0.7	11.8 ± 1.8	− 4.1 ± 0.22 × 10^{-3}	0.94	1.0 ± 0.1 × 10^{-3}	6.9 ± 0.8 × 10^{-4}
0.8	11.4 ± 4.2	− 3.9 ± 0.29 × 10^{-3}	0.95	9.2 ± 1.0 × 10^{-4}	7.3 ± 0.7 × 10^{-4}
0.81	10.2 ± 4.8	− 3.4 ± 0.27 × 10^{-3}	0.96	7.3 ± 1.0 × 10^{-4}	8.1 ± 0.8 × 10^{-4}
0.82	2.2 ± 1.5	− 2.9 ± 0.24 × 10^{-3}	0.97	5.1 ± 0.6 × 10^{-4}	8.6 ± 1.0 × 10^{-4}
0.83	0.3 ± 0.2	− 2.2 ± 0.22 × 10^{-3}	0.98	3.3 ± 0.3 × 10^{-4}	8.7 ± 1.1 × 10^{-4}
0.84	6.7 ± 3.1 × 10^{-2}	− 1.7 ± 0.28 × 10^{-3}	0.99	2.4 ± 0.4 × 10^{-4}	9.4 ± 1.1 × 10^{-4}
0.85	3.4 ± 1.8 × 10^{-2}	− 1.1 ± 0.26 × 10^{-3}	1	8.8 ± 5.9 × 10^{-5}	1.0 ± 0.1 × 10^{-3}
0.86	1.8 ± 0.8 × 10^{-2}	− 5.6 ± 1.9 × 10^{-4}			

Table. S1 Resistivity and TCR of Ag NP thin films according to X_{TBAB} of hybrid ligand exchange.

X_{TBAB}	Br/Ag (atomic ratio)	S/Ag (atomic ratio)
0	0	27.94 (± 2.09)
0.1	1.46 (± 0.83)	21.32 (± 1.91)
0.2	1.82 (± 0.44)	19.22 (± 2.12)
0.3	3.88 (± 1.04)	15.27 (± 1.03)
0.4	3.54 (± 0.55)	12.57 (± 1.47)
0.5	4.99 (± 0.96)	11.54 (± 1.87)
0.6	7.40 (± 0.53)	10.19 (± 1.55)
0.7	10.95 (± 1.88)	7.45 (± 1.13)
0.8	12.59 (± 1.36)	5.37 (± 1.36)
0.9	13.91 (± 1.83)	3.34 (± 0.89)
1	15.75 (± 1.24)	0

Table. S2 Atomic ratio (%) of each element to Ag in the hybrid ligand-exchanged Ag NP thin films with different X_{TBAB} values.

Adsorption site	FCC	HCP	Bridge	Top
E_{ads} (eV)	−1.713	−1.706	−1.673	−1.364

Table. S3 The calculated adsorption energy (E_{ads}) of Br^- on various adsorption sites for the Ag (111) surface.

φ (°)	θ (°)			
	60	90	120	150
30	−2.655	−2.549	−2.527	−2.618
90	−2.603	−2.519	−2.512	−2.614

Table. S4 The calculated adsorption energy (in eV) of MPA on Ag (111) surface as a function of initial angles (θ and ϕ).

Discussion of optical property of each ligand-exchanged Ag NP thin films

UV-vis spectroscopy was performed to examine how the original LSPR absorption peak of Ag NPs changed with each ligand exchange (Fig. S5). For characterization, each ligand-exchanged Ag NP thin film was formed on a glass substrate. For the as-synthesized Ag NPs, the localized surface plasmon resonance (LSPR) absorption peak around 433 nm, which is inherent in Ag NPs, was measured.[1] In the MPA-treated Ag NP thin film, the LSPR peak shifts to 527 nm, which means that the near-field coupling of Ag NPs increases owing to the decrease in inter-particle distance. For TBAB treatment, these LSPR peaks disappear, implying that Ag NPs are sintered into larger particles via physical contact and no longer exhibit LSPR.[2,3] For the hybrid ligand treated, this LSPR peak was found to shift to 506 nm. These LSPR peaks suggest the presence of non-sintered Ag NP arrays inside the thin film. Compared with the peak position of the MPA-treated Ag NP thin films, the red shift was approximately 21 nm less. The difference in peak position is inferred to be because the thin film has a local sintered structure across the Ag NP array, which weakens near-field coupling between the Ag NP arrays.

Discussion of SEM-EDS image and composition analysis

For detailed observation of the surface and cross-section of each ligand-exchanged Ag NP thin film, cross-sectional and vertical SEM images were obtained. The cross-sectional SEM images of the as-synthesized, MPA, TBAB, and hybrid-ligand-treated Ag NP thin films are shown in Fig. S6. The thickness of the as-synthesized Ag NP thin film was approximately 485 ± 14 nm (Fig. S6a). After ligand exchange for MPA, TBAB, and the hybrid ligand with X_{TBAB} = 0.88, the thickness decreased to 172 ± 7, 177 ± 5, and 177 ± 4, respectively. These images show that the characteristics of each ligand exchange were well distinguished. Fig. S6b shows a smooth cross-section packed with MPA-passivated Ag NPs, while Fig. S6c shows a rough cross-section due to the significant growth of Ag NPs by Br^- passivation. The cross section of the hybrid ligand-treated Ag NP thin film (Fig. S6d) shows that locally sintered particles exist between the MPA-passivated Ag NP arrays. The change in thickness of each thin films after ligand exchange is the thickness compression due to the decrease in the interparticle distance and delamination during the rinsing process.

The vertical SEM image and EDS mapping images are shown in Fig. S7. The surface image of the MPA-treated Ag NP thin film was clean without any precipitates, as shown in Fig. S7a. On the other hand, the TBAB-treated Ag NP thin film showed a rough appearance due to the protrusion of the sintered Ag NPs (Fig. S7b).[4] The hybrid ligand-treated Ag NP thin film (Fig. S7c) shows protrusions similar to the case of the TBAB-treated Ag NP thin film, but the scale is smaller. The EDS mapping image of Fig. S7c is shown in Fig. S7d, and it was confirmed that Ag, Br, and S elements at the terminal of the MPA ligand were distributed evenly.

Composition analysis by EDS was performed to quantitatively analyze the ratio of ligands present in each hybrid ligand-exchanged Ag NP thin film.[5] Each sample was prepared by forming an as-synthesized Ag NP thin film on a Si wafer and performing ligand exchange with

X_{TBAB} varying from 0 to 1 at intervals of 0.1. First, the EDS spectra of a single ligand-exchanged Ag NP thin film under the conditions of X_{TBAB} = 0 and 1 were measured and are shown in Figs. S8a-b. The peaks of Br and S were selected to specify each ligand component among the detected Si (1.74 eV), Ag (0.27 keV, 2.9 – 3.2 keV), C (0.54 keV), Br (1.48 keV), and S (2.32 keV) peaks. Fig. S8c shows the EDS spectra recorded for the hybrid ligand-exchanged Ag NP thin films. As X_{TBAB} increased from 0 to 1, the Br peak gradually increased in intensity, while the S peak intensity gradually decreased and disappeared. This confirmed that the amount of ligand passivated to Ag NPs inside the thin film can be controlled by varying the ligand fraction in the hybrid ligand solution. The ratio of each ligand component to the amount of Ag present was plotted against X_{TBAB} by dividing the collected at % of Br and S by the at % of Ag present in each thin film, as shown in Fig. S9. In the MPA-treated and TBAB-treated Ag NP thin films, 28 at% of S and 16 at % of Br were present compared to Ag. This provides a quantitative indication of the amount of passivated ligand on the Ag NP surface. The collected data are presented in Table S2.

Derivation of bond percolation threshold

The bond percolation model was introduced to describe the abrupt change in the electrical resistance of the hybrid ligand-treated Ag NP thin film in terms of the TBAB mole fraction, i.e. X_{TBAB}. The plot of resistance against X_{TBAB} shown in Fig. 1b with a line graph is shown in Fig. S10a. According to percolation theory,[6,7] the electrical conductivity of the hybrid ligand-exchanged Ag NP thin film (σ) in the abrupt change region can be expressed as follows Equation (S1):

$$\sigma(X) = \sigma_{TBAB}(X_{TBAB} - X_{Th})^{t} \quad (X_{TBAB} > x_{Th}) \tag{S1}$$

where σ_{TBAB} is the conductivity of the TBAB treated Ag NP thin film, X_{Th} is the mole fraction of TBAB at the percolation threshold, and t is a critical index related to the dimensionality of the system. In general, in the electrical bond percolation model, the variable appears as the volume fraction of the conducting component. However, in this study, the parameter determining the density of the pathway is X_{TBAB}; therefore, the corresponding value was applied as a variable. Converting it to a resistance parameter with slight modifications is expressed as follows Equation (S2):

$$R(X) = R_{TBAB}(X_{TBAB} - X_{Th})^{-t} \quad (X_{TBAB} > x_{Th}) \tag{S2}$$

The percolation threshold was derived via the differentiation of the abrupt change in the resistance versus X_{TBAB} curve shown in Fig. S10b. The percolation threshold X_{Th} = 0.82 was obtained from the maximum value of the resistance decrease ratio. According to the percolation model, the system yields a straight line by taking the logarithm of equation (S2), and the critical index (t) can be obtained. The logarithm of equation (S2) can be expressed as follows Equation (S3):

$$\log R(X) = \log R_{TBAB} - t \cdot \log \left(X_{TBAB} - X_{Th}\right) \quad \text{(S3)}$$

According to equation (S3), a log-log plot of the measured resistance and $X\text{-}X_{Th}$ values and linear fitting were performed to obtain t = 2.34 and R^2 = 0.977 as shown in Fig. S10c.

References

1 M. Rycenga, C. M. Cobley, J. Zeng, W. Li, C. H. Moran, Q. Zhang, D. Qin, Y. Xia, *Chem. Rev.,* 2011, **111**, 3669.

2 A. T. Fafarman, W. K. Koh, B. T. Diroll, D. K. Kim, D. K. Ko, S. J. Oh, X. Ye, V. Doan-Nguyen, M. R. Crump, D. C. Reifsnyder, C. B. Murray, C. R. Kagan, *J. Am. Chem. Soc.,* 2011, **133**, 15753.

3 A. T. Fafarman, S. Hong, S. J. Oh, H. Caglayan, X. Ye, *ACS Nano,* 2014, **8**, 2746.

4 S. Jeon, J. Ahn, H. Kim, H. K. Woo, J. Bang, W. S. Lee, D. Kim, M. A. Hossain, S. J. Oh, *J. Phys. Chem. C.,* 2019, **123**, 11001.

5 D. E. Newbury, N. W. M. Ritchie, *Scanning,* 2013, **35**, 141.

6 T. Das Gupta, I. Maurin, A. C. H. Rowe, T. Gacoin, *Nanoscale,* 2017, **9**, 3504.Arora, Z. Wang, Z. Jiang, C. R. Chang, H. C. Wu, *Nat. Commun.,* 2021, **12**, 2018.

7 R. Ram, M. Rahaman, A. Aldalbahi, D. Khastgir, *Polym. Int.,* 2017, **66**, 573.